Chemical Science

Accepted Manuscript

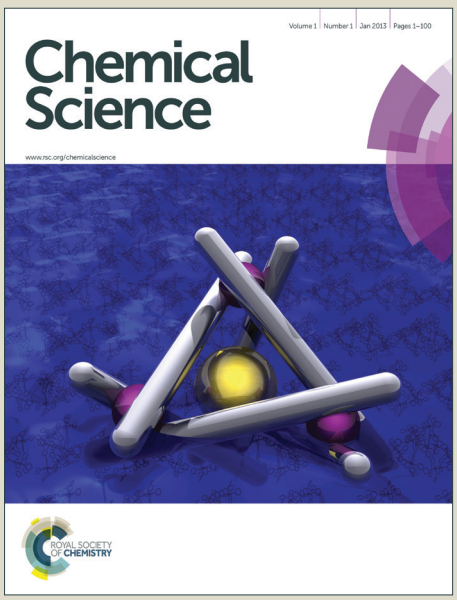

ROYAL SOCIETY OF CHEMISTRY

www.rsc.org/chemicalscience

Chemical Science

RSCPublishing

ARTICLE

Heterolytic Cleavage of H_2 by Bifunctional Manganese(I) Complexes: Impact of Ligand Dynamics, Electrophilicity, and Base Positioning

Elliott B. Hulley,[‡] Monte L. Helm, and R. Morris Bullock*

Cite this: DOI: 10.1039/xoxxoooooox

Received ooth January 20xx,
Accepted ooth January 20xx

DOI: 10.1039/xoxxoooooox

www.rsc.org/

We report the synthesis, characterization, and reactivity with H_2 of a series of Mn^I complexes of the type $[(P\text{-}P)Mn(L_2)CO]^+$ (L_2 = dppm, bppm, or $(CO)_2$; P-P = $P^{Ph}N^{Me}P^{Ph}$ or $P^{Ph}_2N^{Bn}_2$) that bear pendant amine ligands designed to function as proton relays. The pendant amine was found to function as a hemilabile ligand; its binding strength is strongly affected by the ancillary ligand environment around Mn. Tuning the electrophilicity of the Mn center leads to systems capable of reversible heterolytic cleavage of the H–H bond. The strength of pendant amine binding can be balanced to protect the Mn center while still leading to facile reactivity with H_2. Neutral Mn^IH species bearing pendant amines in the diphosphine ligand were found to react with one-electron oxidants and, after proton and electron transfer reactions, regenerate cationic Mn^I species. The reactivity presented herein indicates that the Mn complexes we have developed are a promising platform for development of Mn-based H_2 oxidation electrocatalysts.

Introduction

The coordination and cleavage of molecular hydrogen are fundamentally important reactions that are essential in the reversible conversion of H_2 to protons and electrons.[1-4] This interconversion (Eq. 1) is the cornerstone of efforts towards the development of methods to store and retrieve energy from the H–H bond.

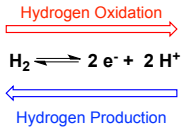

Eq. 1

The investigation of new methods for the utilization of chemical fuels is part of a vital effort to shift towards more sustainable, carbon-neutral energy sources and replace systems based on expensive and unsustainable precious metal catalysts.[5-10] The study of systems that facilitate H–H bond cleavage and formation provides useful information on the interconversion of chemical energy (fuels) and electrical energy. Developing an ensemble of reliable methods for the electrocatalytic oxidation of dihydrogen is particularly critical, as it is the anodic half-reaction in hydrogen fuel cells. In contrast to hydrogen production systems that can be centralized, the consumer side of a future hydrogen economy would ideally be globally distributed and subject to a variety of operating conditions.

Pendant amines that function as proton relays accelerate proton mobility and lower overpotentials in electrocatalytic systems for the production and oxidation of H_2.[2-4, 11, 12] Although different transition metals can vary in the available number of oxidation states, strength of M-H bonds, and geometric changes accompanying redox events, a reliable set of tools for the development of functional electrocatalysts has been developed. We have reported systems for electrocatalytic H_2 production based on Ni[2-4] and Co,[13-15] as well as Ni[16, 17] and Fe-based[18-21] systems for H_2 oxidation. The ability to facilitate and control proton transfer has resulted in significant improvements in electrocatalytic performance, but the enhancements in understanding reveal additional levels of complexity that must be addressed.

Theoretical studies on the Ni-based electrocatalysts for oxidation of H_2 have suggested that the H_2 binding step can be turnover-limiting.[22] Loss of translational motion contributes a significant entropic contribution to this barrier that is not offset by the relatively weak enthalpy of H_2 binding to Ni^{II}. We have focused on developing systems capable of stronger $M(\eta^2\text{-}H_2)$ interaction,[18-21, 23] and we report here our studies on manganese-based systems for H_2 binding and heterolysis.

Manganese is an attractive metal for electrocatalyst development due to its abundance, relatively low cost and toxicity, and a wide variety of observed oxidation states (Mn^{VII} – Mn^{-I}).[24] Kubas and coworkers discovered that cationic $[Mn^I(diphosphine)_2(CO)]^+$ complexes reversibly bind H_2,[25-28] suggesting a convenient platform for investigation of Mn-mediated H_2 heterolysis. In contrast to systems based on Co and Ni, diphosphine ligands bound to Mn^I are considerably less labile, and synthetic pathways have been developed for facile synthesis of heteroleptic complexes. The ability to synthesize complexes with just one ligand containing a pendant amine is important, as proton control strategies can be developed that are essentially independent of electronic control at Mn (Figure 1).

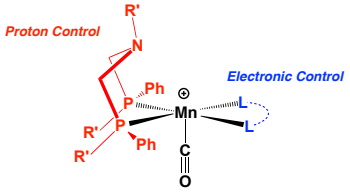

Figure 1. Design strategy for Mn-based electrocatalysts bearing proton relays, showing a 16-electron Mn(I) fragment.

We recently reported a study of the cationic Mn^{I} complex $[(\kappa^3\text{-}P^{Ph}_2N^{Bn}_2)Mn(CO)(bppm)]^+[BAr^F_4]^-$ ($P^{Ph}_2N^{Bn}_2$ = 1,5-dibenzyl-3,7-diphenyl-1,5-diaza-3,7-diphosphacyclooctane, bppm = $(PAr^F_2)_2CH_2$, Ar^F = 3,5-$(CF_3)_2C_6H_3$) and its reactivity with H_2 at low temperature.[23] The structure of the P_2N_2 ligand and electrophilic nature of the Mn resulted in the formation of a stable κ^3-complex, wherein the amine coordinates to the Mn center. Pendant base coordination is reversible; solutions of the cation reacted rapidly with H_2 and suggest rapid $\kappa^2 \leftrightharpoons \kappa^3$ equilibrium as depicted in Figure 2. In this case, not only was intramolecular heterolysis of H_2 favorable and reversible, but exceedingly rapid proton and hydride exchange was observed (>15,000 s^{-1} at –95 ºC). This exchange, which presumably operates via an intermediate $Mn(\eta^2\text{-}H_2)$ complex, occurs with a very low barrier (< 6.8 kcal mol^{-1}) and indicates that although the product of heterolytic cleavage (with an Mn-H and N-H bond) is favored, its equilibrium with the $Mn(\eta^2\text{-}H_2)$ adduct approaches thermoneutrality.

Coordination of the pendant base has significant implications for H_2 oxidation electrocatalysis in this system, and can influence design strategies for future systems using pendant base-containing ligands bound to electrophilic metals. Pendant amine binding has not been observed in comparable Ni and Co systems, but has been previously observed it with $(\kappa^3\text{-}P^{Ph}_2N^{Bn}_2)CrCl_3$,[29] and Rauchfuss and co-workers reported related κ^3-binding of an azadithiolate ligand in a [FeFe]-hydrogenase model complex.[30] Rauchfuss proposed that redox-triggered reversibility of this κ^3-interaction could explain reversible oxidative deactivation of [FeFe]-hydrogenase, although subsequent computational investigations have suggested that steric repulsion by the protein scaffold minimizes the strength of the nascent Fe-N bond in the native protein.[31] In the present system, dissociation of the amine and the generation of a coordinatively unsaturated metal center likely precedes H_2 binding; we are thus interested in studying how ligand designs can affect the availability of this coordination site. We have developed amine-bearing diphosphines that differ in their ability to interact with metal-bound H_2. The PNP class of ligands typically have chair conformation in the ground state, and must first undergo a ring flip to the boat conformer to position the pendant amine close to the metal center.[32-35] The P_2N_2 class of ligands, with the substituents on phosphorus constrained in a macrocycle, usually adopt a geometry that has one pendant amine properly positioned for such interactions (Figure 3). This relatively simple change in ligands allows a direct examination and comparison of the issues of pendant amine binding and intramolecular H–H heterolysis.

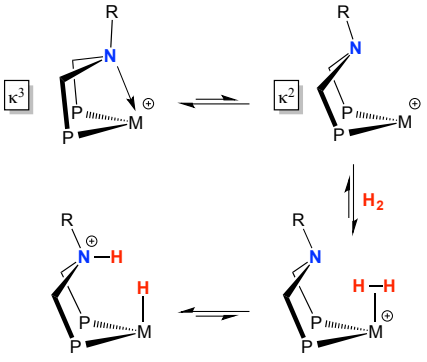

Figure 2. Amine dissociation, H_2 coordination, and H–H heterolysis in a bifunctional metal complex.

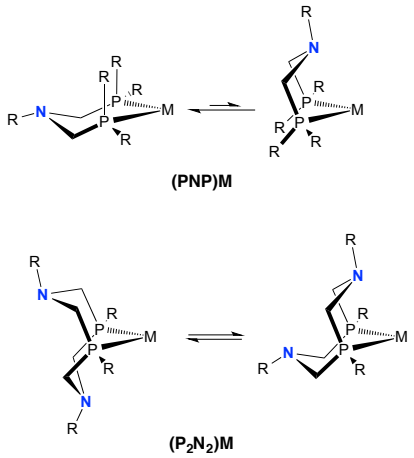

Figure 3. Pendant base positioning in complexes of PNP and P_2N_2 ligands.

Herein, we report a study of the stability, pendant base hemilability, and reactivity with H_2 of a series of cationic Mn complexes containing both classes of diphosphine ligands (PNP and P_2N_2).

Results

Syntheses of Mn(I) Cationic Complexes.

Cationic Mn complexes bearing the $P^{Ph}_2N^{Bn}_2$ ligand were prepared by halide abstraction. The bromide in the complex $(P^{Ph}_2N^{Bn}_2)Mn(Br)(CO)_3$ (**1-Br**) is sufficiently labile that the reaction with excess $NaBAr^F_4$ in fluorobenzene (PhF) is rapid (< 5 min) at 22 ºC, affording solutions of the cationic complex $[(\boldsymbol{\kappa^3}\text{-}P^{Ph}_2N^{Bn}_2)Mn(Br)(CO)_3]^+$ (**1[κ³]⁺**). The previously reported cations $[(\boldsymbol{\kappa^3}\text{-}P^{Ph}_2N^{Bn}_2)Mn(CO)(dppm)]^+$ (**2[κ³]⁺**) and $[(\kappa^3\text{-}P^{Ph}_2N^{Bn}_2)Mn(CO)(bppm)]^+$ (**3[κ³]⁺**) are similarly prepared from analogous bromide precursors as $BAr^F_4{}^-$ salts (Scheme 1).[36] A single resonance for each of these cationic species was observed when the abstraction reactions were monitored by ^{31}P NMR spectroscopy.

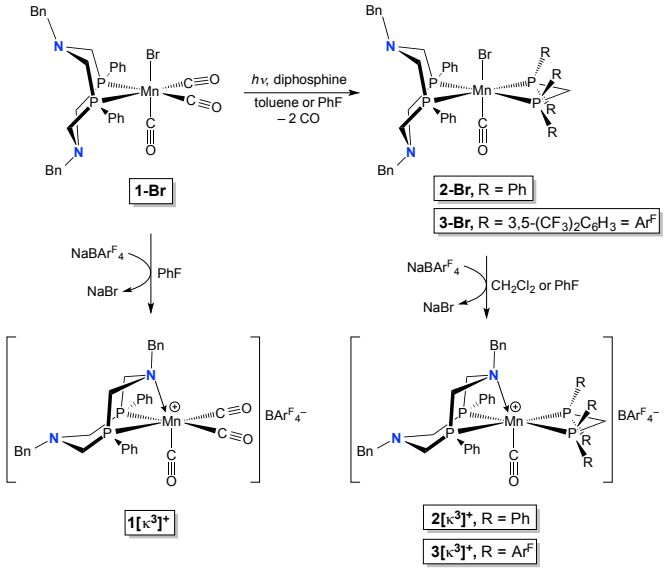

Scheme 1. Synthesis of cationic complexes **1[κ³]⁺**, **2[κ³]⁺** and **3[κ³]⁺** from **1-Br**.

Table 1. Differences in ^{31}P NMR Chemical Shifts Between Tuck-in Species **1[κ^3]$^+$** – **5[κ^3]$^+$** and their Precursors **1-Br** – **5-Br** in [(P-P)Mn(L$_2$)CO]$^+$.

L_2	P-P	^{31}P shift (ppm) of [(P-P)MnBr]	^{31}P shift (ppm) of [(κ^3-P-P)Mn]$^+$	Δδ (ppm)
dppm	$P^{Ph}_2N^{Bn}_2$	29.8 (**2-Br**)	23.7 (**2[κ^3]$^+$**)	–6.1
bppm	$P^{Ph}_2N^{Bn}_2$	28.9 (**3-Br**)	18.4 (**3[κ^3]$^+$**)	–10.5
bppm	$P^{Ph}_2N^{Me}$	21.3 (**4-Br**)	15.7 (**4[κ^3]$^+$**)	–5.6
$(CO)_2$	$P^{Ph}_2N^{Bn}_2$	28.9 (**1-Br**)	–4.5 (**1[κ^3]$^+$**)	–33.4
$(CO)_2$	$P^{Ph}_2N^{Me}$	20.9 (**5-Br**)	–3.5 (**5[κ^3]$^+$**)	–24.4

The κ^3-coordination indicated in Scheme 1 is assigned on the basis of ^{31}P NMR spectroscopy and was confirmed by X-ray crystallography. The ^{31}P NMR resonances for the P_2N_2 ligands of **1[κ^3]$^+$**, **2[κ^3]$^+$** and **3[κ^3]$^+$** are shifted upfield relative to their bromide precursors (Table 1), characteristic of the ^{31}P nuclei being part of a four-membered ring.[37] This shift is most pronounced for **1[κ^3]$^+$** (Δδ 33.4 ppm) , whereas the changes in chemical shifts are more modest for **2[κ^3]$^+$** (Δδ 6.1 ppm) and **3[κ^3]$^+$** (Δδ 5.6 ppm).

Variable-temperature NMR studies of **3[κ^3]$^+$** (presented below) strongly suggest the κ^3-interaction is dominant in solution, and it seems likely that is also the case for **2[κ^3]$^+$**. The solid-state molecular structures of **2[κ^3]$^+$** and **3[κ^3]$^+$** are presented in Figure 4, wherein the ligand framework has been truncated to highlight the κ^3-binding mode of the $P^{Ph}_2N^{Bn}_2$ ligand (selected metrical parameters are presented in Table S1 in the ESI).

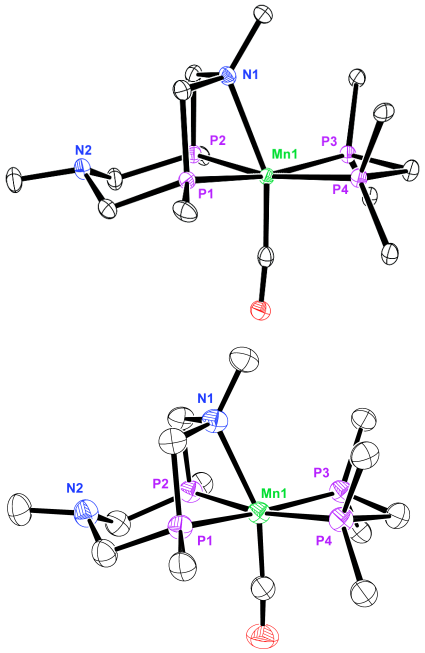

Figure 4. Solid-state structures of (κ^3-$P^{Ph}_2N^{Bn}_2$)Mn(CO)(dppm)$^+$ (**2[κ^3]$^+$**, at –173 °C) and (κ^3-$P^{Ph}_2N^{Bn}_2$)Mn(CO)(bppm)$^+$ (**3[κ^3]$^+$**, at –73 °C) (50% probability ellipsoids). Substituents on the P and N have been truncated, and hydrogen atoms, $BAr^F_4^-$, and co-crystallized CH_2Cl_2 have been omitted for clarity.

Both **2[κ^3]** and **3[κ^3]** exhibit distorted octahedral geometry, wherein the N-Mn-CO bond angles deviate from the expected 180° (158.1(1)º and 158.10(8)º, respectively). There is a slight contraction of the Mn-N bond in **3[κ^3]$^+$** relative to **2[κ^3]$^+$** (2.290(2) Å vs. 2.316(3) Å), although both of these Mn-N bond distances are considerably longer than a typical Mn^I-N(sp^3) bond (2.17(5) Å, from analysis of 26 structures in the Cambridge Structural Database, see ESI).

In contrast to the $P^{Ph}_2N^{Bn}_2$ derivatives, the Mn^I compounds containing the $P^{Ph}N^{Me}P^{Ph}$ ligand were not amenable to simple halide abstraction approaches. Treatment of ($P^{Ph}N^{Me}P^{Ph}$)MnBr(CO)(bppm) (**4-Br**) with $NaBAr^F_4$ in PhF at 22 °C for several days failed to yield observable abstraction products, and heating the solution led to the appearance of multiple products including free bppm, indicating decomposition of the cation under these conditions. However, treatment of a red PhF solution of **4-Br** with $NaBAr^F_4$ and H_2 (1 atm, 22ºC) for two days led to conversion to a yellow solution of **4-H/NH$^+$**, the product of heterolytic cleavage of H_2 (Scheme 2). Addition of ^{i}Pr$_2$NEt readily deprotonated **4-H/NH$^+$** to give **4-H**. The intermediacy **4-H/NH$^+$** was confirmed by preparing it independently (see below). Single crystals of both **4-Br** and **4-H** were isolated, and their solid-state structures are presented in Figure 5.

Treatment of red-orange **4-H** with $[Ph_3C]^+[B(C_6F_5)_4]^-$ in PhF resulted in the formation of a green solution containing equimolar amounts of the target cation (as isomers **4[κ^2]$^+$** and **4[κ^3]$^+$** in a 2:1 ratio) and **4-H/NH$^+$** (Figure 6). The identity of the tuck-in isomer **4[κ^3]$^+$** was assigned by the upfield shift of the ^{31}P NMR resonance of the PNP ligand (15.7 ppm), whereas **4[κ^2]$^+$** was assigned based on the similarity to the previously published dppm analog [($P^{Ph}N^{Me}P^{Ph}$)Mn(CO)(dppm)].[36] Gomberg's dimer was observed as a product by NMR spectroscopy,[38-40] implying that the trityl cation oxidized **4-H** to the radical cation [($P^{Ph}N^{Me}P^{Ph}$)Mn^{II}H(CO)(bppm)]$^+$ (**[4-H]$^+$**), followed by further reactions of **[4-H]$^+$** to give the observed Mn^I products depicted in Figure 6. Although direct hydride transfer from metal hydrides to $[Ph_3C]^+$ is often observed,[41-43] $[Ph_3C]^+$ can serve as a one-electron oxidizing agent, especially in cases of easily oxidized metal hydrides or those where bulky ligands may prevent close approach of $[Ph_3C]^+$ to the M-H bond.[44]

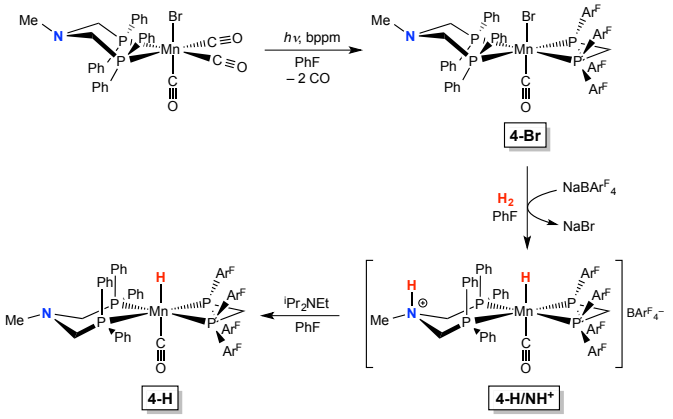

Scheme 2. Synthesis of **4-Br**, **4-H/NH$^+$** and **4-H** from ($P^{Ph}N^{Me}P^{Ph}$)Mn(Br)(CO)$_3$.

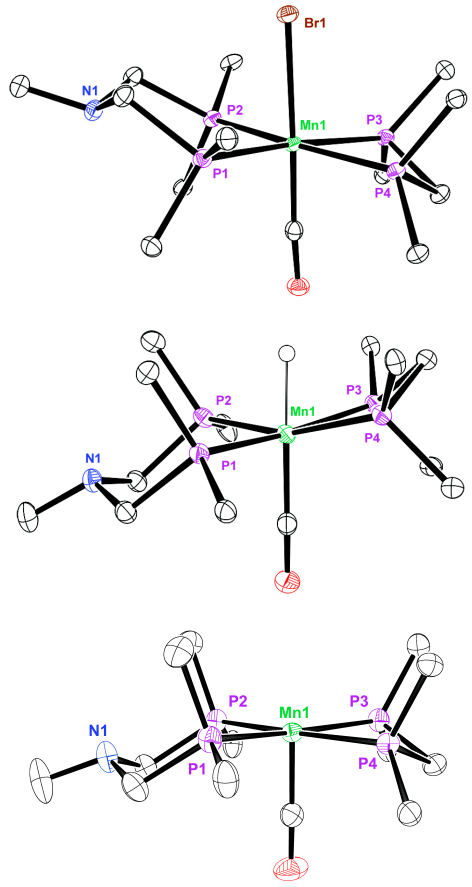

Figure 5. Solid-state molecular structures of ($P^{Ph}N^{Me}P^{Ph}$)Mn(Br)(bppm)(CO) (**4-Br**, at –173 °C), ($P^{Ph}N^{Me}P^{Ph}$)MnH(bppm)(CO) (**4-H**, at –133 °C) and [(κ^2–$P^{Ph}N^{Me}P^{Ph}$)Mn(Br)(bppm)(CO)]$^+$[BAr^F_4]$^-$ (**4[κ^2]$^+$[BAr^F_4]$^-$**, at –133 °C) (50% probability ellipsoids). Substituents on the P and N have been truncated, and carbon-bound hydrogen atoms, the counteranion for **4[κ^2]$^+$**, and co-crystallized solvent have been omitted for clarity.

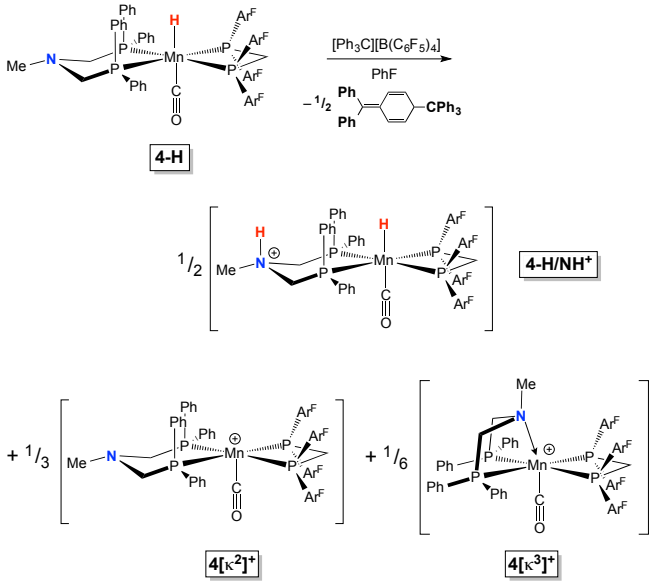

Figure 6. Oxidation of **4-H** to yield a mixture of **4-H/NH**$^+$ and isomers **4[κ^2]**$^+$ and **4[κ^3]**$^+$. The anion is $B(C_6F_5)_4^-$.

Slowly degassing the solution results in elimination of H_2 from **4-H/NH**$^+$ over the course of ~10 minutes and >80% conversion ($^{31}P\{^1H\}$ NMR spectroscopy) to **4[κ^2]**$^+$ and **4[κ^3]**$^+$ as a blue-green solution. The complex **4[κ^2][$B(C_6F_5)_4$]** has a low solubility in PhF; over the course of 12 h, deep blue crystals precipitate from the **4-H/NH**$^+$/**4[κ^2]**$^+$/**4[κ^3]**$^+$ mixture; they were amenable to X-ray crystallographic analysis and were identified as **4[κ^2][$B(C_6F_5)_4$]** (Figure 5). The blue color of solid **4[κ^2][$B(C_6F_5)_4$]** is considerably more intense than the blue/green solution it precipitated from, and implies that, like **1[κ^3]**$^+$–**3[κ^3]**$^+$, the tuck-in species **4[κ^3]**$^+$ is yellow/orange in color. When crystalline **4[κ^2][$B(C_6F_5)_4$]** is redissolved in PhF, $^{31}P\{^1H\}$ NMR signals attributed to **4[κ^2]**$^+$ and **4[κ^3]**$^+$ are regenerated in a 2:1 ratio.

As with **4-Br**, preparation of the $P^{Ph}N^{Me}P^{Ph}$ analog of **1[κ^3]**$^+$ directly by halide abstraction was unsuccessful. Treatment of ($P^{Ph}N^{Me}P^{Ph}$)Mn(Br)(CO)$_3$ with either $NaBAr^F_4$, AgOTf or $TlPF_6$ in PhF resulted in complex product mixtures. In the hope of adapting the strategy that proved successful for **4-H**, the tricarbonyl hydride **5-H** was prepared by treatment of ($P^{Ph}N^{Me}P^{Ph}$)Mn(Br)(CO)$_3$ with $LiAlH_4$. Although the cation **5[κ^3]**$^+$ can be prepared from **5-H** by oxidation with $[Ph_3C][B(C_6F_5)_4]$, the product salt is generated as an amorphous solid. We were thus unable to crystallize **5[κ^3]**$^+$ away from byproducts generated via this route. Instead, **5-H** was oxidized by an equivalent of silver triflate to generate **5-OTf** as a crystalline solid in 71% yield, which readily produced the cationic species **5[κ^3]**$^+$ upon addition of $NaBAr^F_4$ in PhF solution (Scheme 3). Although the salt **5[κ^3]**$^+$[BAr^F_4]$^-$ is also an amorphous solid, the triflate abstraction proceeds very cleanly. As with **1[κ^3]**$^+$, there is no evidence of the κ^2 isomer in solution.

The structure and stereochemistry of **5-OTf** was confirmed by X-ray crystallography and the solid-state structure is presented in the ESI. (Figure S1). As with **1[κ^3]**$^+$, there is a substantial upfield shift in the ^{31}P NMR resonance of the $P^{Ph}N^{Me}P^{Ph}$ ligand from **5-OTf** (20.5 ppm) to **5[κ^3]**$^+$ (–3.5 ppm) diagnostic of the four-membered phosphacycle.

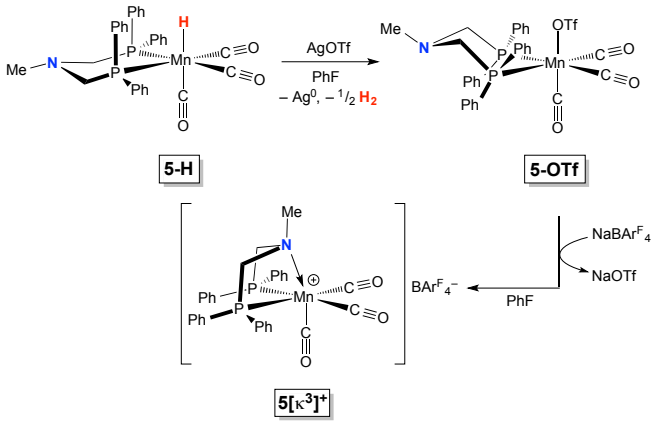

Scheme 3. Synthesis of **5-OTf** and **5[κ^3]**$^+$ from **5-H** via oxidation and triflate abstraction.

Dynamics of Pendant Amine Coordination

The tuck-in Mn cations **1[κ³]**$^+$ – **5[κ³]**$^+$ vary greatly in the lability of their bound pendant amines. The $Mn(CO)_3$ species **1[κ³]**$^+$ and **5[κ³]**$^+$ both show sharp singlets in their ^{31}P NMR spectra at 25 ºC and show only minor changes in linewidth at elevated temperatures (65ºC, PhF). In contrast, the ^{31}P NMR spectra for **2[κ³]**$^+$, **3[κ³]**$^+$, and **4[κ²]**$^+$/**4[κ³]**$^+$ at 25 ºC exhibit broad resonances that suggest dynamic processes are occurring.

Variable temperature and 2D NMR studies of **3[κ³]**$^+$ reveal that the Mn-N interaction is indeed labile, but also suggest that the dynamic processes are not limited to simple dissociation to give a 16-electron Mn complex. The $^{31}P\{^1H\}$ NMR spectrum of **3[κ³]**$^+$ in CD_2Cl_2 solution at low temperature (< 0 ºC) manifests as a pair of second-order multiplets at 18.4 ppm and 31.0 ppm (for the P_2N_2 and bppm ligands, respectively). When heated in a sealed NMR tube from –7 ºC to 81 ºC, the ^{31}P resonance of the P_2N_2 signal of **3[κ³]**$^+$ broadens considerably, while shifting downfield, and then begins to coalesce at 20.8 ppm. Careful inspection of the low-temperature spectra revealed the presence of a resonance at 63 ppm (Figure S2) that changed in breadth and relative intensity with temperature, as expected for a dynamic process approaching the intermediate exchange rate regime. Moreover, the weighted average of the small (~5% at –47 ºC) peak at 63 ppm and the 18.4 ppm signal for **3[κ³]**$^+$ is consistent with the modest positive shift seen towards coalescence. Integration of the $^{31}P\{^1H\}$ NMR resonances at 63 ppm and 18.4 ppm from –47 ºC to –3 ºC allowed the determination of thermodynamic parameters via van't Hoff analysis (Figure S3). From these data, a significant negative entropy change (ΔS^o = –10(2) cal mol^{-1} K^{-1}) accompanies isomerization of the κ³-complex; this entropy change is seemingly inconsistent with the entropy increase expected for simple amine dissociation.

Further spectroscopic studies suggest that the observed dynamism is due to the participation of an agostic complex (**3[κ³$_{agostic}$]**$^+$), wherein the apical benzylic methylene donates a C–H bond to the Mn center. Exchange spectroscopy (EXSY) experiments at –15 ºC revealed that the ^1H NMR signal for the apical benzylic protons (at 2.32 ppm) was in chemical exchange with a minor species at –1.66 ppm (Figure S4), consistent with the expected upfield shift of an agostic interaction.[45, 46] Since only one C–H bond of the benzylic methylene group can interact with the 5-coordinate Mn center at a time, the observed chemical shift represents the average environment of a benzylic proton (3-5 ppm) and an agostic proton (–4 to –7 ppm).[46] The loss of symmetry and conformational flexibility in **3[κ³$_{agostic}$]**$^+$ could explain the entropy loss determined by van't Hoff analysis.

In order to obtain kinetic information about this process, the variable-temperature ^{31}P NMR data were simulated and rate constants were extracted. The spectra could be modeled as two species undergoing non-mutual exchange; a selection of the experimental and simulated spectra is presented in Figure 7. Using the chemical shifts of **3[κ³$_{agostic}$]**$^+$ and **3[κ³]**$^+$ and their relative abundances calculated from the van't Hoff analysis, rate constants for exchange of the two species were determined by non-linear least-squares fitting to the experimental spectra. A summary of the kinetic and thermodynamic data pertaining to the **3[κ³$_{agostic}$]**$^+$ and **3[κ³]**$^+$ exchange is presented in Figure 8. Having realized the nature of ligand positioning must play a significant role in this type of dynamics, we turned our attention to the "non-positioned" PNP system.

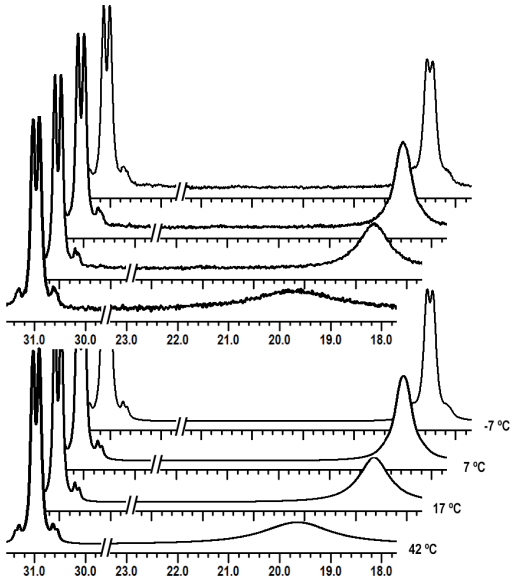

Figure 7. Selected experimental (top) and simulated (bottom) $^{31}P\{^1H\}$ NMR spectra of solutions of **3[κ³]**$^+$ from –7 ºC to 42 ºC in CD_2Cl_2. Resonances on the right correspond to the P_2N_2 ligand; resonances on the left correspond to the bppm ligand.

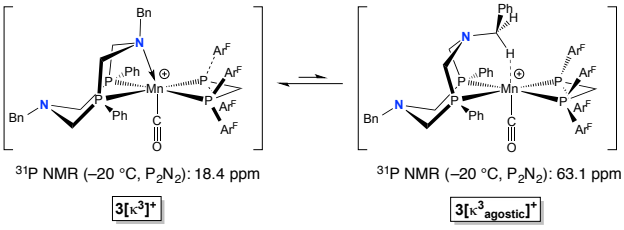

Figure 8. The equilibrium between **3[κ³]**$^+$ and **3[κ³$_{agostic}$]**$^+$, with energies derived from equilibrium studies and kinetic modeling indicated.

The ligand dynamics in the PNP derivative **4[κ²]**$^+$ indicate that interconversion between κ² and κ³ isomers is rapid on the NMR timescale, thus the observed 2:1 ratio reflects their equilibrium distribution (i.e., the κ²-isomer is more stable than the κ³-isomer, Figure 9). EXSY spectra ($^{31}P\{^1H\}$ observed) recorded at –15 ºC of the **4[κ³]**$^+$/**4[κ²]**$^+$ equilibrium mixture (Figure S5) revealed chemical exchange between the two species. Although low solubility of **4[κ²]**$^+$ in PhF prevented in depth study, lineshape analysis of the $^{31}P\{^1H\}$ NMR spectra collected at 20 ºC and –15 ºC allow the estimation of the rate of **4[κ³]**$^+$ ⇋ **4[κ²]**$^+$ interconversion to be on the order of 10^2 –10^3 s^{-1} at 20 ºC (Figure S6).

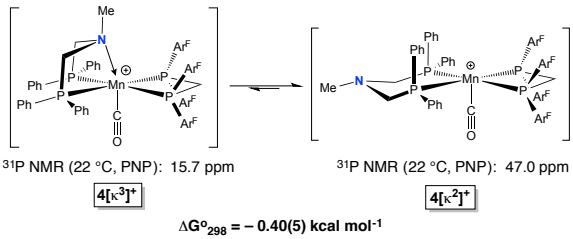

Figure 9. The interconversion between **4[κ³]**$^+$ and **4[κ²]**$^+$, with free energy derived from equilibrium studies indicated. The anion is $B(C_6F_5)_4^-$.

Reactivity of [(P-P)Mn(CO)L$_2$]$^+$ Species with H$_2$.

The cationic Mn complexes discussed above (**1[κ^3]**$^+$ – **5[κ^3]**$^+$) differ substantially in their ability to bind and heterolytically cleave H$_2$. The reaction of **2[κ^3]**$^+$ with hydrogen results in facile reversible formation of an η^2-H$_2$ adduct, as discussed in our previous study.[36] In contrast, addition of hydrogen to solutions of the more electron-deficient **3[κ^3]**$^+$ (in PhF or CD_2Cl_2) results in the formation of the protonated hydride *syn,endo*-**3-H/NH**$^+$ (Figure 10) without the observable formation of an intermediate η^2-H$_2$ adduct.[23] Heterolysis of H$_2$ is fully reversible; removal of the H$_2$ atmosphere results in complete conversion back to **3[κ^3]**$^+$. At low temperature (≤ –20 ºC) a single product is observed by ^{1}H and ^{31}P NMR spectroscopies, and 2D NMR spectroscopic studies reveal the species to be consistent with an *endo*-protonated Mn hydride, wherein the proton and hydride environments rapidly exchange and manifest as a single peak.

Upon warming to room temperature, two isomers of *syn,endo*-**3-H/NH**$^+$ appear, as evidenced by new hydride resonances at –4.83 and –5.61 ppm. Knowledge of the structure and stereochemistry of *syn,endo*-**3-H/NH**$^+$ and multiple 2D-NMR techniques allows the assignment of the likely structures for the other two isomers. The proposed structures for these species are presented in Figure 10, and the relevant portions of the ^{1}H, ^{31}P, and ^{15}N NMR spectra are presented in Figures S7-S9. The hydride resonance at –5.61 ppm integrates 1:1 with a new resonance at 13.33 ppm, consistent with an NH. Using ^{1}H,^{15}N-HSQCADTOXY correlation spectroscopy on the ^{15}N-labeled isomer mixture revealed a third NH at 7.31 ppm (Figure S10), and ^{2}H NMR spectra of the analogous deuteride isomer mixture (not ^{15}N-labeled), prepared by addition of D$_2$ to **3[κ^3]**$^+$ at room temperature, revealed an ND at this shift (7.3 ppm) that integrated 1:1 with an MnD at –4.8 ppm (Figure S11). A summary of the NMR spectroscopic data assigned to *syn,endo*–**3-H/NH**$^+$ is presented in Figure 11.[47] At equilibrium (established within minutes and unchanged after several hours), the isomers *syn,endo*-**3-H/NH**$^+$, *syn,exo*-**3-H/NH**$^+$, and *anti,endo*-**3-H/NH**$^+$, are in a 1 : 1.3 : 0.1 ratio.

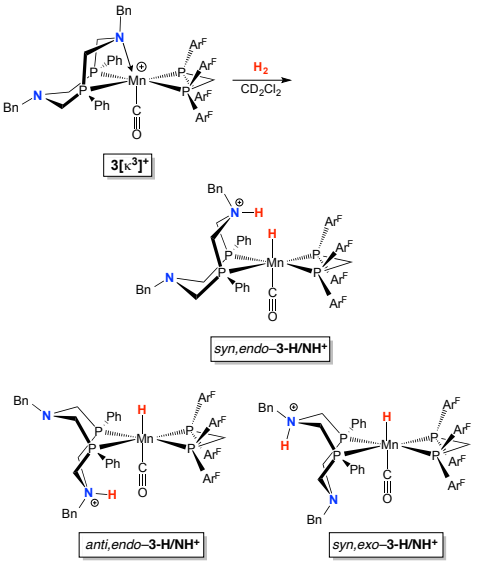

Figure 10. Proposed structures for the three major isomeric products of heterolytic H$_2$ cleavage. *Syn* and *anti* refer to the position of the proton relative to the hydride about the P$_4$ plane while *endo* and *exo* refer to the directionality of the N–H bond vector towards or away (respectively) the H–Mn–CO axis.

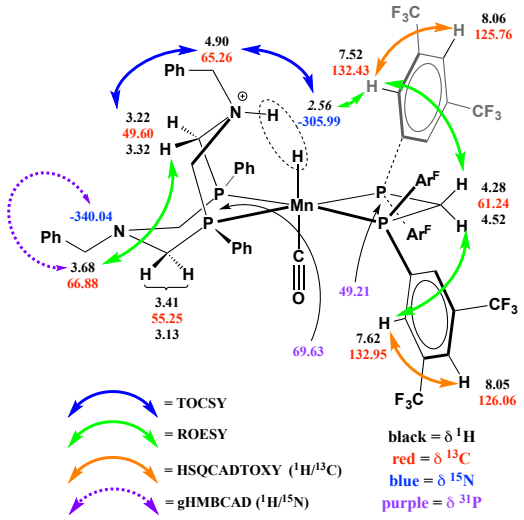

Figure 11. Compilation of selected multinuclear 1D and 2D-NMR spectral data assigned to ***syn,endo*-3-H/NH**$^+$.[48] (Ar^F = 3,5-(CF$_3$)$_2$C$_6$H$_3$)

The overall thermodynamic favorability of H$_2$ binding and cleavage by the PNP complex **4[κ^2]**$^+$ is likely similar to that of the P$_2$N$_2$ analog **3[κ^2]**$^+$, but the single pendant base simplifies the product distribution. Addition of H$_2$ to a suspension of **4[κ^2]**$^+$ in PhF solution resulted in an immediate color change from blue to yellow, with concomitant dissolution of **4[κ^2]**$^+$. The ^{31}P NMR spectrum of the yellow solution reveals a single species, observed previously from oxidation of **4-H** (Figure 6), that we assign to be *syn*-**4-H/NH**$^+$. When the PhF solvent is removed under vacuum and replaced with d$_5$-PhBr, crystals of [*syn*-**4-H/NH**$^+$][B(C$_6$F$_5$)$_4$]•(d$_5$-PhBr) begin to deposit within minutes. Crystals suitable for X-ray diffraction were isolated directly from an NMR tube used for spectroscopic studies; the solid-state structure is presented in Figure 12. At low temperatures (–30 ºC) another hydride resonance at –2.5 ppm is observable in low abundance (~10% of *syn*-**4-H/NH**$^+$) that we assign as the isomer with inverted protonation stereochemistry, *anti*-**4-H/NH**$^+$ (Figure 13). A related set of protonated FeH complexes, [(P^{Et}N^{Me}HP^{Et})Fe**H**(L)(dppm)]$^+$ (L = CO, CH$_3$CN), has been previously described and shows similar protonation isomerism.[33] The linewidth of the hydride resonance at –2.5 ppm is temperature dependent, and below –30 ºC is not observable. This is presumably due to some sort of dynamic process; although ring-flip dynamics are an attractive possibility for the origin of this behavior (see Discussion), intermolecular exchange cannot be ruled out with the available data.[49]

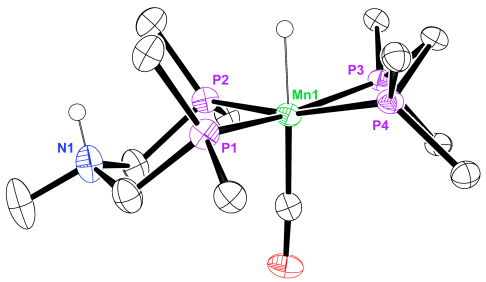

Figure 12. Solid-state structure of ***syn*-4-H/NH**$^+$ (at –123 °C) (50% probability ellipsoids). Substituents on the P and N have been truncated, and hydrogen atoms, the B(C$_6$F$_5$)$_4$ anion, and co-crystallized d$_5$-PhBr have been omitted for clarity.

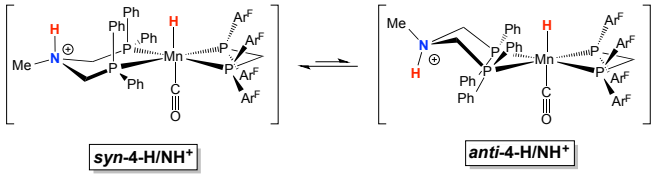

Figure 13. Structure and interconversion of protonation isomers of **4-H/NH**$^+$. *Syn* and *anti* refer to the position of the proton relative to the hydride about the P_4 plane. The anion is $B(C_6F_5)_4^-$.

Similar to *syn,endo*-**3-H/NH**$^+$, the proton and hydride environments of *syn*-**4-H/NH**$^+$ undergo exchange. The exchange can be frozen out, and the NH (4.35 ppm) and MnH (–3.23 ppm) chemical shifts can be independently observed at –42 ºC (500 MHz). Although well below the coalescence temperature, the NH chemical shift is obscured by ligand resonances at temperatures above –40 ºC (Figure S13). A single peak for the NH/MnH positions is observed above 40 ºC, with the proton and hydride environments averaging to a peak (integrating for 2H) at 0.43 ppm. The ^{1}H NMR spectra from –41 ºC to 62 ºC were simulated (Figure S16) using a mutual exchange model, and the extracted rate constants were used to determine activation energetics via Eyring analsysis (Figure S17). The activation parameters, presented in Figure 14, indicate proton/hydride exchange occurs at a rate of 9.7×10^3 s^{-1} at 20 ºC.

In contrast to the rich H_2 reactivity described above, the tricarbonyl species **1**$[\kappa^3]^+$ and **5**$[\kappa^3]^+$ are unreactive with H_2 (1 atm) after weeks at 22 ºC. When isolated **1-H** or **5-H** are treated with $[H(OEt_2)_2][B(C_6F_5)_4]$ in PhF solution, there is rapid evolution of gas (presumably H_2) and the generation of the corresponding κ^3-complex (observed by ^{31}P NMR), indicating the lack of reactivity with H_2 is thermodynamic in origin. Although such a strong acid raises questions of the site of kinetic protonation (i.e. pendant amine vs. hydride ligand),[50, 51] the analysis of *syn,endo*-**3-H/NH**$^+$ and *syn,endo*-**4-H/NH**$^+$ (see Discussion) implies that deprotonation of a bound H_2 ligand should be rapid and competitive with H_2 elimination.

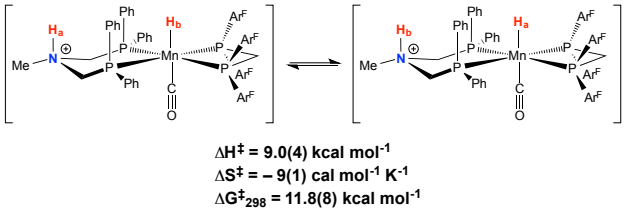

Figure 14. Degenerate exchange of proton and hydride positions in ***syn*-4-H/NH**$^+$, with activation parameters derived from Eyring analysis of rates calculated from NMR simulations. The anion is $B(C_6F_5)_4^-$.

Discussion

Ligand Dynamics and their Impact on Reactivity

Understanding the nature of the Mn-N bond in the tuck-in complexes **1**$[\kappa^3]^+$–**5**$[\kappa^3]^+$ is critical to using its lability in potential catalytic reactions. Although the increased electrophilicity of Mn in **3**$[\kappa^3]^+$ (relative to dppm analog **2**$[\kappa^3]^+$) results in a slightly shorter Mn-N bond, both interactions are likely weak. As can be seen in Figure 4, the N-Mn-C 158.10(8)° angle deviates sharply from the 180º expected for octahedral geometry, indicating significantly reduced σ-overlap with the d-orbitals. Part of the lability of these bonds is thus caused by the relief of ring strain imposed by the geometry of the P_2N_2 ligand, but space-filling models of both **2**$[\kappa^3]^+$ and **3**$[\kappa^3]^+$ (Figure S18) suggest there is also considerable repulsion between the apical benzyl group of the P_2N_2 ligand and the ancillary chelating diphosphine (dppm or bppm).

When comparing the ^{31}P NMR chemical shifts of tuck-in species **1**$[\kappa^3]^+$–**5**$[\kappa^3]^+$ to their bromide precursors **1-Br**–**5-Br** (Results, Table 1), there is a clear increase in the upfield shift as the electrophilicity of the complexes is increased (i.e., for P-P = $P_2^{Ph}N_2^{Bn}$, Δδ increases as dppm < bppm < $(CO)_2$). The Mn atoms in tricarbonyl cations **1**$[\kappa^3]^+$ and **5**$[\kappa^3]^+$ are substantially more exposed than in **2**$[\kappa^3]^+$–**4**$[\kappa^3]^+$, and the N-donors can approach with minimal steric repulsion. In the absence of experimental molecular structures for **1**$[\kappa^3]^+$, **4**$[\kappa^3]^+$, and **5**$[\kappa^3]^+$, these species were investigated computationally so that the structural impact of amine binding could be compared across the series (computed structures shown in Figure S19). The Mn-N distances are calculated to be substantially shorter in **1**$[\kappa^3]^+$ and **5**$[\kappa^3]^+$ (2.204 Å and 2.209 Å, respectively) than in **2**$[\kappa^3]^+$–**4**$[\kappa^3]^+$, with significant consequences for the bond angles about the phosphorus atoms; NMR chemical shifts of ^{31}P nuclei are known to be sensitive to the bond angles about the P atom.[52] The lack of reactivity of **1**$[\kappa^3]^+$ and **5**$[\kappa^3]^+$ with H_2 further supports that the Mn-N bonds are stronger in these species than in **2**$[\kappa^3]^+$–**4**$[\kappa^3]^+$.

Our exploration of the dissociation dynamics in **3**$[\kappa^3]^+$ provides a more comprehensive understanding of the interaction of pendant amines with metal centers. Simulation of the variable-temperature NMR data allowed us to determine activation parameters, lending more experimental evidence for the proposed **3**$[\kappa^3_{\text{agostic}}]^+$ structure. For the conversion from **3**$[\kappa^3]^+$ to **3**$[\kappa^3_{\text{agostic}}]^+$ the entropy change ($\Delta S^\ddagger = -10(4)$ cal mol^{-1} K^{-1}), although associated with a rather large estimated error, is inconsistent with the positive entropy change expected for simple dissociation of the pendant amine to yield a 5-coordinate complex. The modest enthalpy change ($\Delta H_{298} = -1.0(2)$ kcal mol^{-1}) suggests that the stabilization provided by the κ^3-amine is comparable to that afforded by the agostic interaction. DFT calculations were again employed in order to gain support for the assignment of **3**$[\kappa^3_{\text{agostic}}]^+$ as the minor isomer of **3**$[\kappa^3]^+$. Such a structure was found as a minimum (Figure 15a) and solvent-corrected thermochemical calculations (1 atm, 25 ºC) placed **3**$[\kappa^3_{\text{agostic}}]^+$ 1.60 kcal mol^{-1} above **3**$[\kappa^3]^+$, in good agreement with the experimental value (2.0(2) kcal mol^{-1}). The structure of **3**$[\kappa^3_{\text{agostic}}]^+$ can be thought of as arising from inversion of the κ^3-nitrogen with concomitant movement of the benzyl group towards the Mn center. The unsaturated, 16-electron isomer **3**$[\kappa^2]^+$ (Figure 15b) lies 3.9 kcal mol^{-1} above **3**$[\kappa^3]^+$ in free energy (c.f. **4**$[\kappa^3]^+ \leftrightharpoons$ **4**$[\kappa^2]^+$, $\Delta G = -0.40(5)$ kcal mol^{-1}). Since an open coordination site is necessary for H_2 coordination, **3**$[\kappa^2]^+$ is a required intermediate and must be energetically accessible. The addition of H_2 to **3**$[\kappa^3]^+$ is known to be kinetically facile (>95% conversion in seconds), thus the calculated energy of **3**$[\kappa^2]^+$ agrees with experiment. The computational and experimental studies of the ligand dynamics in and H_2 cleavage by **3**$[\kappa^3]^+$ are summarized graphically in Figure 16.

Interactions with C–H bonds have been previously reported for cationic Mn complexes. Agostic interactions,[45, 46] formally described as covalent 3-center-2-electron bonds between a C–H bond and a transition metal, have been observed for $(PCy_3)_2Mn(CO)_3^+$ wherein the H•••C distance is 2.01(9) Å.[27]

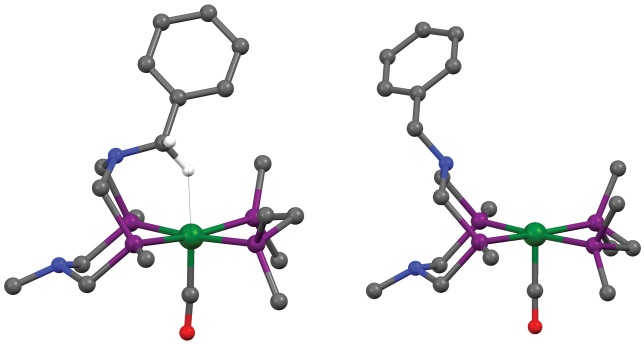

Figure 15. Computed structures of cations (a) $\mathbf{3[\kappa^3_{agostic}]^+}$ and (b) $\mathbf{3[\kappa^2]^+}$. Hydrogen atoms (except for the agostic CH_2), substituents on phosphorus, and the *anti* benzyl group have been truncated for clarity.

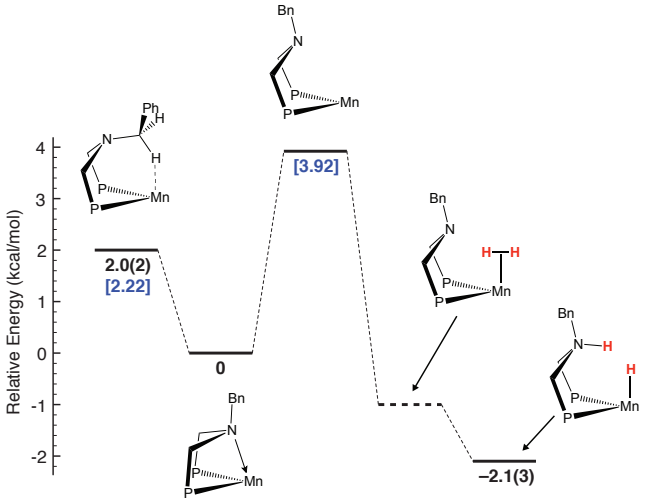

Figure 16. Free energy diagram of the intermediates involved in pendant amine dissociation from and H_2 heterolysis by $\mathbf{3[\kappa^3]^+}$. Experimental values are listed in black and computed values in [blue]. The *minimum* relative energy of $\mathbf{3\text{-}(\eta^2\text{-}H_2)}$ is inferred from isotopic labeling experiments as described in the text.

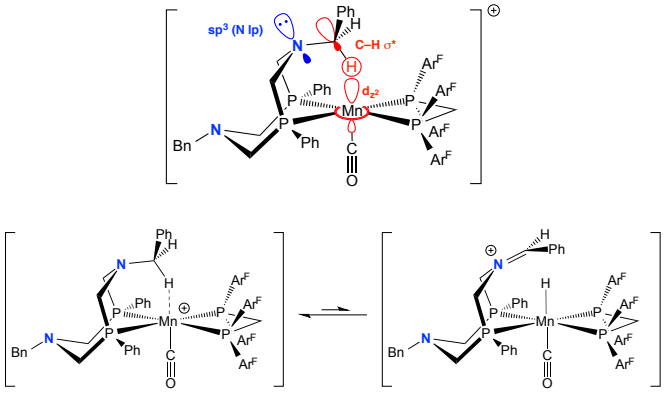

Figure 17. Negative hyperconjugation interactions stabilize the agostic C–H in $\mathbf{3[\kappa^3_{agostic}]^+}$ (top); intramolecular hydride transfer to Mn resulting in formation of an iminium cation (bottom).

Anagostic interactions,[46] which are typically weaker and electrostatic in nature, have been previously observed in cationic bis(diphosphine) Mn complexes. Kubas reported significant M•••H interactions in $(\kappa^2\text{-}PR_2CH_2CH_2PR_2)_2Mn(CO)^+$ (R = Et, Ph; Mn•••H distances of ~3.3 Å and 2.89(6) Å, respectively),[26] and our previous study of $(P^{Ph}N^{Me}P^{Ph})_2Mn(CO)(dppm)^+$ revealed an anagostic interaction (2.7562(3) Å).[36] A related M•••H interaction was previously reported by our group in the complex $(P^{tBu}_2N^{Bn}_2)Ni(CH_3CN)_2^{2+}$ (Ni•••H distance of 2.56 Å),[13] which is consistent with a weak *anagostic* interaction; the C–H interaction in the calculated structure of $\mathbf{3[\kappa^3_{agostic}]^+}$ is clearly agostic (Mn•••H distance of 1.964 Å).

Although the DFT calculations indicate that the binding energies of the amine in $\mathbf{3[\kappa^3]^+}$ and the agostic C–H $\mathbf{3[\kappa^3_{agostic}]^+}$ are both modest, it is surprising that the binding of the pendant amine is of comparable strength to that of the agostic benzyl group. The geometry of the agostic benzyl group places the agostic CH-bond *anti* to the amine lone-pair, providing a possible explanation for the unusual stability. NBO analysis[53] indicates substantial donation from the lone pair on N to the CH σ*-orbital, suggesting that at least part of the strength of the agostic bond in $\mathbf{3[\kappa^3_{agostic}]^+}$ is due to hydridic character on H (details in ESI). This hydridic character can be thought of as arising from negative hyperconjugation[54-56] of the lone pair on the apical pendant amine to the adjacent unfilled C–H σ*-orbital (Figure 17, top). Agostic interactions are commonly described in terms of the donation of a *filled orbital of a C–H bond* into an empty d-orbital;[46, 57] in the present case the carbon appears to be significantly less involved than in "traditional" agostic interactions, as negative hyperconjugation would tend to stabilize electron density on the *hydrogen atom* by partially filling the carbon valence. Strong $N(sp_3)\rightarrow C\text{–}H(\sigma^*)$ donation would result in formal hydride transfer to Mn, and this agostic interaction might be better represented as resonance structures as in Figure 17 (bottom). This type of donation manifests in the calculated structure as a shortening of the apical benzylamine C–N bond length (1.432 Å) relative to that in the non-agostic benzyl group (1.471 Å); for comparison, the C–N bond lengths within the P_2N_2 macrocycle differ by considerably smaller amounts (1.451 ± 0.002 Å). Alkyl amines are known to act as hydride donors,[58,59] and it is possible that negative hyperconjugation interactions contribute to this type of reactivity. The ability of the electrophilic Mn to accept a hydride is a key factor in the strength of the agostic bond, as well as H–H heterolysis (see below).

Pendant amine binding to the metal center has a significant impact on the chemical stability of the cationic species. Like other electrophilic metal complexes, unsaturated Mn^I complexes are usually reactive with CH_2Cl_2. The CH_2Cl_2 sensitivity of the series we present here correlates with the lability of the Mn-N bond. Whereas the tricarbonyl species $\mathbf{1[\kappa^3]^+}$ and $\mathbf{5[\kappa^3]^+}$ are stable for weeks in CH_2Cl_2 solution, $\mathbf{3[\kappa^3]^+}$ suffers 50% decomposition within a week and $\mathbf{4[\kappa^2]^+}$ reacts within seconds. The latter is particularly sensitive; PhF solutions of $\mathbf{4[\kappa^2]^+}$ in sealed vials inside an argon-filled glovebox decompose in a matter of days. The exact pathway of this decomposition is unknown, but the *trans*-dicarbonyl $\mathbf{4[CO]^+}$ was isolated from decomposed batches as a yellow crystalline solid and was characterized by X-ray crystallography (Figure S20). This compound can also be readily prepared independently from adding gaseous CO to solutions of $\mathbf{4[\kappa^2]^+}$. The substantial π-backbonding in $\mathbf{4[\kappa^2]^+}$

(ν_{CO} = 1854 cm^{-1}) suggests that initial dissociation of CO by thermal means is unlikely, and that instead an adventitious impurity first oxidizes the complex followed by CO loss and trapping via an equivalent of **4[κ²]**$^+$. Similar decomposition products were reported by Kubas.[26] This proposed pathway is supported by the observation that **4[CO]**$^+$ is detectable, sometimes in substantial quantities (~10%), in NMR experiments where **4[κ²]**$^+$ is prepared *in situ* by oxidation of **4-H**. Clearly, the stability imparted by the tuck-in interaction in **3[κ³]**$^+$ appears to kinetically protect it from such decomposition pathways.

Reversible Heterolytic Cleavage of H_2; Impacts of Structural Reorganization on Rapid Proton/Hydride Exchange

The exchange of proton and hydride environments in *syn*-**4-H/NH**$^+$, although rapid, is considerably slower than in *syn*-**3-H/NH**$^+$. The differences between these two systems highlight the inherent kinetic advantages in the positioned- (P_2N_2) vs. non-positioned (PNP) bases. The barrier for proton/hydride exchange in *syn*-**3-H/NH**$^+$ is exceptionally low; indeed, since decoalescence was never observed, we could only estimate an upper bound on the barrier (< 6.8 kcal mol^{-1} at –95 ºC).[23] We were unable to directly measure the rate at multiple temperatures. In contrast, the exchange in *syn*-**4-H/NH**$^+$ is so much slower that the activation parameters for this process can be determined. From these activation parameters we calculate a $\Delta G^{\ddagger}_{298}$ of 11.8(8) kcal mol^{-1}, corresponding to a rate of 9.7 × 10^3 s^{-1} at 20 ºC (cf. >10^7 at 20 ºC for *syn*-**3-H/NH**$^+$). Thus, although poor base positioning inhibits the rate of exchange by a factor of *at least* 10^3, it is notable that the limiting factor in the heterolysis of the strong H–H bond is a ring flip.

The entropy cost to generate the activated complex for proton/hydride exchange in *syn*-**4-H/NH**$^+$ ($\Delta S^{\ddagger}$ = –9(1) cal mol^{-1} K^{-1}) is indicative of a significant loss of disorder from the ground state structure. This is consistent with the need for two fundamental steps; conformational change of the six-membered ring from chair to boat, bringing the protonated amine into proximity of the hydride ligand, and then the reversible protonation of the hydride to yield the η^2-H_2 complex (Figure 18). Although it is not currently known which step is rate-determining, the overall barrier is of similar magnitude to chair/boat isomerism measured in related Ni systems.[60, 61] However, as shown in Figure 18, the chair isomer of *syn*-**4-H/NH**$^+$ is both structurally and electronically very similar to *syn,endo*-**3-H/NH**$^+$, and thus $\Delta H^{\ddagger}$ and $\Delta S^{\ddagger}$ for the proton exchange step will likely be similar to that in *syn*-**3-H/NH**$^+$.

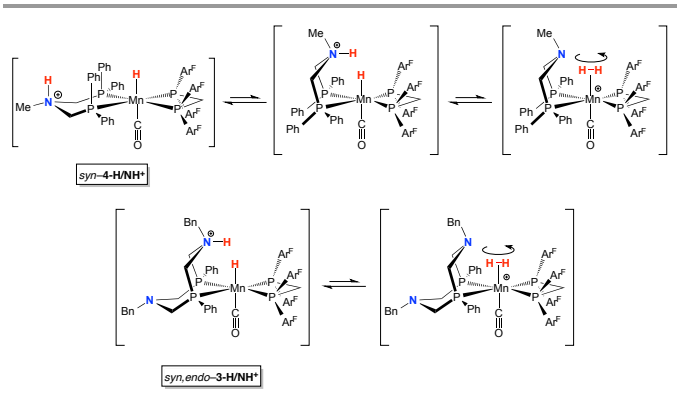

Figure 18. Structure and bond change considerations for proton/hydride exchange in ***syn*-4-H/NH**$^+$ (top) and ***syn,endo*-3-H/NH**$^+$ (bottom).

The rapid activation of H_2 in *syn,endo*-**3-H/NH**$^+$ is reminiscent of (but distinct from), the polyhydrides of the type $M(H)(H_2)$ and $M(H)_2(H_2)$.[62-64] These systems, which possess H–H activation barriers that are less than 5 kcal mol^{-1}, could be thought of as heterolytic activations in which the hydride deprotonates the adjacent H_2 ligand (σ-bond metathesis). This is likely not the best description, however, as there is significant homolytic character in the sense that metal d-orbitals mediate the exchange (i.e. oxidative-addition/reductive-elimination).[65] The fact that the bond rearrangements are mediated by the same center places these reactions in a different class from that of the bifunctional systems involving the critical role of pendant amines described in the present work. Since there is no change in redox state of the Mn, the bifunctional heterolytic activation is much more akin to H–H activation accomplished by Frustrated Lewis Pairs (FLPs),[66-69] and theoretical studies on FLPs provide an appropriate means of understanding the present system.

The great facility with which proton/hydride exchange occurs *syn,endo*-**3-H/NH**$^+$ may be due to both the rigid framework of the complex as well as the energy matching of *syn,endo*-**3-H/NH**$^+$ and **3-(η²-H₂)**). Prior to our report of *syn,endo*-**3-H/NH**$^+$, experimental studies on bifunctional H_2 heterolysis had found only moderate rates of activation under ambient conditions (10^{-3}–10^4 s^{-1}),[33, 70, 71] although computational work had suggested that this mode of activation could proceed with very little barrier. In a computational study of H_2 activation by $[Ni(P^{Cy}_2N^{Me}_2)_2]^{2+}$,[22] Raugei *et al.* determined that the transition state for heterolytic H_2 cleavage from the high-energy intermediate $[Ni(P^{Cy}_2N^{Me}_2)_2(\eta^2\text{-}H_2)]^{2+}$ was on the order of only 5 kcal mol^{-1}. Heterolytic cleavage of H_2 was found to be assisted by the polarization of the binding pocket created by the electrophilic Ni^{2+} center and the positioned pendant amine nucleophile, and that the overall barrier to H_2 cleavage by $[Ni(P^{Cy}_2N^{Me}_2)_2]^{2+}$ was dominated by the entropic cost of binding H_2 to Ni. In a related theoretical study on heterolytic H_2 splitting by the FLP model system NH_3/BCl_3,[72] Camaioni *et al.* computed the barrier for heterolytic scission in the *pre-associated* NH_3-H_2-BCl_3 complex to be 7.9 kcal mol^{-1}. The transition state structure showed little H–H bond scission, indicating an early transition state, and significant pyramidalization of the BCl_3 fragment. Formation of the product $[NH_4^+][HBCl_3^-]$ requires significant geometric reorganization of the BCl_3 fragment, and decomposition analysis of the transition state showed that significant *electronic* reorganization is also essential along the path to products. In both of these systems, however, it is the entropic costs due to H_2 binding and/or pre-association that dominate the overall barrier to cleavage. In the present system, the substantial H_2 binding energy and rigid ligand environment ensure that there is minimal reorganization energy on the path from **3-(η²-H₂)** to *syn,endo*-**3-H/NH**$^+$.

The close H–H distance in *syn,endo*-**3-H/NH**$^+$ (~1.5 Å)[23,73] suggests a dihydrogen bonding interaction,[21,74] and raises questions the nature of proton/hydride exchange mechanism. Quantum mechanical (QM) effects such as exchange coupling[62] and tunneling have a substantial distance dependence and might play a substantial role in the observed proton/hydride exchange. In this context, QM exchange coupling refers to an effect observed in ^{1}H NMR spectra of some transition metal polyhydrides wherein anomalously large J_{HH} couplings are observed between the protons of adjacent (but magnetically inequivalent) hydride ligands. These large couplings have been found to be due to a QM exchange process, mediated by

tunneling, and many of these exchange-coupled hydrides possess H–H distances between 1.4 Å – 1.6 Å. Significant QM exchange might suggest that mutual tunneling of protons would provide a mechanism for proton/hydride exchange that *does not* involve an intermediate H_2 complex.

Exchange coupling is not detectable in the available data due to the magnetic equivalence of the MnH and NH environments in *syn,endo*-**3-H/NH**$^+$, but isotopic labeling studies provide evidence that tunneling is not a key factor in the observed rapid proton/hydride exchange. When **3[κ^3]**$^+$ is treated with HD, the singly-deuterated isotopomer of *syn,endo*-**3-H/NH**$^+$ is formed wherein the deuterium is rapidly exchanged between MnD and ND positions.[23] Rapid H/D exchange is observable down to –95 ºC, as observed by the strong temperature dependence of the ^{1}H chemical shift for the MnH/NH average signal. As H/D exchange approached the slow exchange limit one would expect normal decoalescence behavior, e.g. broadening and splitting of the MnH/NH average signal into distinct MnH and NH resonances, but this is not observed. Since the proton and deuteron are quantum mechanically distinct and cannot be included in the same nuclear wavefunction, a mutual exchange pathway is not possible. It is entirely possible that this pathway is operative for *syn,endo*-**3-H/NH**$^+$, but it is clear that this would be an additional effect that occurs in a system that is *already* capable of very facile heterolysis of H_2. It still feasible that tunneling plays a role in producing the Mn(η^2-HD) intermediate complex, but this is related to the fact that the activation barrier is already low. In fact, the possibility of tunneling thus further highlights the advantages that can be gained by energy-matching strategies.

Towards Mn-Based Electrocatalysts for H_2 Oxidation

Having established a detailed understanding of the ligand dynamics and H_2 reactivity of a series of Mn complexes, we have a solid framework for developing H_2 oxidation electrocatalysts. Essentially all of the required reactions necessary for turnover in electrocatalytic oxidation of H_2 (Figure 19) are directly or indirectly invoked in the chemistry we have presented here. Coordination and heterolysis of H_2 is clearly favorable and facile for **3[κ^2]**$^+$ and **4[κ^2]**$^+$, as well as subsequent deprotonation to generate a neutral MnH. Completion of the cycle and regeneration of the Mn cation requires the removal of two electrons and a proton; chemical oxidation of **4-H** rapidly yields **4[κ^2]**$^+$/**4[κ^3]**$^+$ and *syn*-**4-H/NH**$^+$ (Figure 20), indicating the intermolecular proton and electron transfer events such as those depicted in Figure 19 are operative and potentially electrochemically detectable. Such studies are ongoing and will be reported separately.

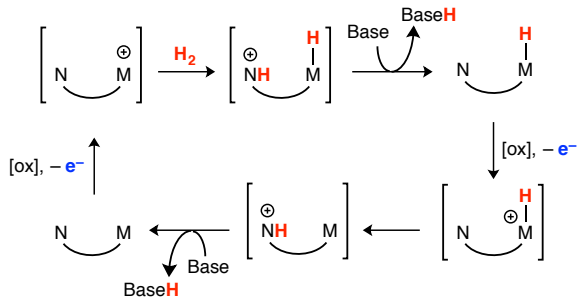

Figure 19. One possible reaction sequence for electrocatalytic oxidation of H_2 by a bifunctional catalyst.

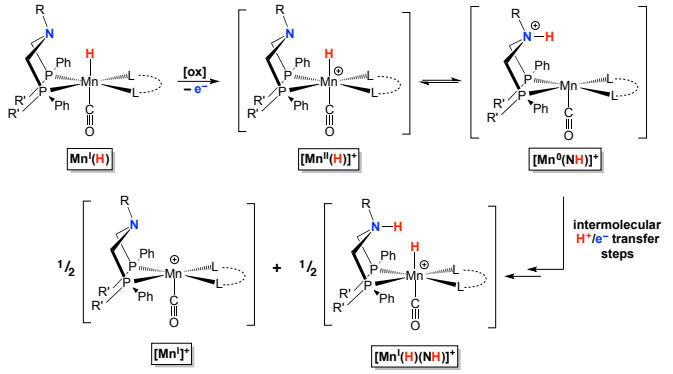

Figure 20. One possible mechanism for regeneration of Mn^I species following oxidation of a Mn^{I}H complex.

Conclusion

We found that, in contrast to related Ni and Co systems, the pendant amine readily binds to the Mn center; the favorability of amine binding depends on the electrophilicity of the Mn center, the steric bulk around the apical coordination site, and nature of pendant base positioning. When these factors are balanced through the use of the bppm ligand, the Mn^I centers are sufficiently electrophilic that heterolytic cleavage of H_2 is favorable and facile. Moreover, coordination of the amine in [(κ^3-P$^{Ph}_2$N$^{Bn}_2$)Mn(CO)(bppm)]$^+$ confers a degree of stability towards CH_2Cl_2, a solvent that rapidly decomposes the unprotected analog [(κ^2-P^{Ph}N^{Me}P^{Ph})Mn(CO)(bppm)]$^+$, without hindering H_2 reactivity. In both the P_2N_2 and PNP variants, the proton/hydride and Mn(η^2-H_2) forms are close in energy and the MnH and NH moieties engage in rapid intramolecular exchange via Mn(η^2-H_2). Starting from [(κ^3-P$^{Ph}_2$N$^{Bn}_2$)Mn(CO)(bppm)]$^+$, the species involved in binding and heterolytically cleaving H_2 span only a ~6 kcal mol^{-1} free energy range, indicating a very promising platform for the development of a new family of H_2 oxidation electrocatalysts. Stoichiometric studies of H_2 reactivity and oxidation have shown promising results and indicate that electrocatalytic H_2 oxidation is feasible.

Acknowledgements

We are grateful to Dr. Aaron M. Appel, Dr. Neeraj Kumar, and Dr. Jonathan Darmon for thoughtful discussions. The research was supported as part of the Center for Molecular Electrocatalysis, an Energy Frontier Research Center funded by the U.S. Department of Energy, Office of Science, Office of Basic Energy Sciences. Pacific Northwest National Laboratory is operated by Battelle for DOE.

Notes and references

[a] Center for Molecular Electrocatalysis, Physical Sciences Division, Pacific Northwest National Laboratory, P.O. Box 999, K2-57, Richland, Washington 99352
‡ Current address: Department of Chemistry, Box 3838, University of Wyoming, Laramie, Wyoming 82071

† Electronic Supplementary Information (ESI) available: Experimental procedures, computational details, and Supplementary Figures S1-S20. CCDC 1008334–1008340. See DOI: 10.1039/b000000x/

References

1. S. Ogo, *Chem. Commun.*, 2009, 3317-3325.
2. D. L. DuBois and R. M. Bullock, *Eur. J. Inorg. Chem.*, 2011, 1017-1027.
3. D. L. DuBois, *Inorg. Chem.*, 2014, **53**, 3935-3960.
4. R. M. Bullock, A. M. Appel and M. L. Helm, *Chem. Commun.*, 2014, **50**, 3125-3143.
5. R. M. Bullock, Ed., *Catalysis Without Precious Metals*, Wiley-VCH: Weinheim, 2010.
6. E. Alonso, F. R. Field and R. E. Kirchain, *Environmental Science & Technology*, 2012, **46**, 12986-12993.
7. V. S. Thoi, Y. Sun, J. R. Long and C. J. Chang, *Chem. Soc. Rev.*, 2013, **42**, 2388-2400.
8. P. Du and R. Eisenberg, *Energy. Environ. Sci.*, 2012, **5**, 6012-6021.
9. M. Wang, L. Chen and L. Sun, *Energy Environ. Sci.*, 2012, **5**, 6763-6778.
10. R. H. Crabtree, *New J. Chem.*, 2011, **35**, 18-23.
11. J. Y. Yang, R. M. Bullock, W. J. Shaw, B. Twamley, K. Fraze, M. Rakowski DuBois and D. L. DuBois, *J. Am. Chem. Soc.*, 2009, **131**, 5935–5945.
12. M. Rakowski DuBois and D. L. DuBois, *Acc. Chem. Res.*, 2009, **42**, 1974-1982.
13. E. S. Wiedner, J. Y. Yang, W. G. Dougherty, W. S. Kassel, R. M. Bullock, M. Rakowski DuBois and D. L. DuBois, *Organometallics*, 2010, **29**, 5390-5401.
14. E. S. Wiedner, J. A. S. Roberts, W. G. Dougherty, W. S. Kassel, D. L. DuBois and R. M. Bullock, *Inorg. Chem.*, 2013, **52**, 9975-9988.
15. E. S. Wiedner, A. M. Appel, D. L. DuBois and R. M. Bullock, *Inorg. Chem.*, 2013, **52**, 14391-14403.
16. J. Yang, S. Chen, W. G. Dougherty, W. S. Kassel, R. M. Bullock, D. DuBois, S. Raugei, R. Rousseau, M. Dupuis and M. Rakowski DuBois, *Chem. Commun.*, 2010, **46**, 8618-8620.
17. J. Y. Yang, S. E. Smith, T. Liu, W. G. Dougherty, W. A. Hoffert, W. S. Kassel, M. Rakowski DuBois, D. L. DuBois and R. M. Bullock, *J. Am. Chem. Soc.*, 2013, **135**, 9700-9712.
18. T. Liu, S. Chen, M. J. O'Hagan, M. Rakowski DuBois, R. M. Bullock and D. L. DuBois, *J. Am. Chem. Soc.*, 2012, **134**, 6257-6272.
19. T. Liu, D. L. DuBois and R. M. Bullock, *Nat. Chem.*, 2013, **5**, 228-233.
20. J. M. Darmon, S. Raugei, T. Liu, E. B. Hulley, C. J. Weiss, R. M. Bullock and M. L. Helm, *ACS Catal.*, 2014, **4**, 1246-1260.
21. T. Liu, X. Wang, C. Hoffmann, D. L. DuBois and R. M. Bullock, *Angew. Chem. Int. Ed.*, 2014, **53**, 5300-5304.
22. S. Raugei, S. Chen, M.-H. Ho, B. Ginovska-Pangovska, R. J. Rousseau, M. Dupuis, D. L. DuBois and R. M. Bullock, *Chem. Eur. J.*, 2012, **18**, 6493-6506.
23. E. B. Hulley, K. D. Welch, A. M. Appel, D. L. DuBois and R. M. Bullock, *J. Am. Chem. Soc.*, 2013, **135**, 11736-11739.
24. N. N. Greenwood and A. Earnshaw, *Chemistry of the Elements*, Butterworth-Heinemann, Oxford, UK, 1997.
25. X. Fang, J. Huhmann-Vincent, B. L. Scott and G. J. Kubas, *J. Organomet. Chem.*, 2000, **609**, 95–103.
26. W. A. King, B. L. Scott, J. Eckert and G. J. Kubas, *Inorg. Chem.*, 1999, **38**, 1069-1084.
27. A. Toupadakis, G. J. Kubas, W. A. King, B. L. Scott and J. Huhmann-Vincent, *Organometallics*, 1998, **17**, 5315-5323.
28. W. A. King, X.-L. Luo, B. L. Scott, G. J. Kubas and K. W. Zilm, *J. Am. Chem. Soc.*, 1996, **118**, 6782-6783.
29. M. T. Mock, S. Chen, R. Rousseau, M. J. O'Hagan, W. G. Dougherty, W. S. Kassel, D. L. DuBois and R. M. Bullock, *Chem. Commun.*, 2011, **47**, 12212-12214.
30. M. T. Olsen, T. B. Rauchfuss and S. R. Wilson, *J. Am. Chem. Soc.*, 2010, **132**, 17733-17740.
31. T. Miyake, M. Bruschi, U. Cosentino, C. Baffert, V. Fourmond, C. Léger, G. Moro, L. Gioia and C. Greco, *J. Biol. Inorg. Chem.*, 2013, **18**, 693-700.
32. C. J. Curtis, A. Miedaner, R. Ciancanelli, W. W. Ellis, B. C. Noll, M. Rakowski DuBois and D. L. DuBois, *Inorg. Chem.*, 2003, **42**, 216-227.
33. R. M. Henry, R. K. Shoemaker, D. L. DuBois and M. Rakowski DuBois, *J. Am. Chem. Soc.*, 2006, **128**, 3002-3010.
34. R. M. Henry, R. K. Shoemaker, R. H. Newell, G. M. Jacobsen, D. L. DuBois and M. Rakowski DuBois, *Organometallics*, 2005, **24**, 2481-2491.
35. G. M. Jacobsen, R. K. Shoemaker, M. Rakowski DuBois and D. L. DuBois, *Organometallics*, 2007, **26**, 4964-4971.
36. K. D. Welch, W. G. Dougherty, W. S. Kassel, D. L. DuBois and R. M. Bullock, *Organometallics*, 2010, **29**, 4532-4540.
37. P. E. Garrou, *Chem. Rev.*, 1981, **81**, 229-266.
38. H. Lankamp, W. T. Nauta and C. MacLean, *Tetrahedron Lett.*, 1968, **9**, 249-254.
39. J. M. McBride, *Tetrahedron*, 1974, **30**, 2009-2022.
40. M. Gomberg, *J. Am. Chem. Soc.*, 1900, **22**, 757-771.
41. T.-Y. Cheng, B. S. Brunschwig and R. M. Bullock, *J. Am. Chem. Soc.*, 1998, **120**, 13121-13137.
42. T.-Y. Cheng and R. M. Bullock, *J. Am. Chem. Soc.*, 1999, **121**, 3150-3155.
43. T.-Y. Cheng and R. M. Bullock, *Organometallics*, 2002, **21**, 2325-2331.
44. T.-Y. Cheng, D. J. Szalda, J. Zhang and R. M. Bullock, *Inorg. Chem.*, 2006, **45**, 4712-4720.
45. M. Brookhart, M. L. H. Green and L.-L. Wong, *Prog. Inorg. Chem.*, 1988, **36**, 1-124.
46. M. Brookhart, M. L. H. Green and G. Parkin, *Proc. Natl. Acad. Sci. U.S.A.*, 2007, **104**, 6908-6914.
47. A detailed explanation of the spectroscopic investigations used to assign the connectivity of the proposed syn,exo and anti,endo isomers is presented in the ESI.
48. Nuclear assignments for protons directly bound to carbon and nitrogen were made via ^{1}H/^{13}C-HSQCAD and ^{1}H/^{15}N-HSQCAD, respectively. Assignments for ^{31}P nuclei were made by ^{1}H,^{31}P-gHMBCAD correlations to ligand protons and ^{1}H,^{31}P-HSQCAD correlations to the hydride protons.
49. Although observable, this species is a very minor component and full spectral characterization was not pursued.
50. M. Besora, A. Lledós and F. Maseras, *Chem. Soc. Rev.*, 2009, **38**, 957.
51. G. Eilers, L. Schwartz, M. Stein, G. Zampella, L. De Gioia, S. Ott and R. Lomoth, *Chem. Eur. J.*, 2007, **13**, 7075-7084.
52. D. Purdela, *J. Magn. Reson.*, 1971, **5**, 23-36.
53. E. D. Glendening, A. E. Reed, J. E. Carpenter and F. Weinhold.
54. W. Scherer, P. Sirsch, D. Shorokhov, G. S. McGrady, S. A. Mason and M. G. Gardiner, *Chem. Eur. J.*, 2002, **8**, 2324-2334.
55. L. Perrin, L. Maron, O. Eisenstein and M. F. Lappert, *New J. Chem.*, 2002, **27**, 121-127.
56. V. I. Minkin, *Pure Appl. Chem.*, 1999, **71**, 1919-1981.
57. E. F. van der Eide, P. Yang and R. M. Bullock, *Angew. Chem. Int. Ed.*, 2013, **52**, 10190-10194.
58. A. F. Pozharskii, M. A. Povalyakhina, A. V. Degtyarev, O. V. Ryabtsova, V. A. Ozeryanskii, O. V. Dyablo, A. V. Tkachuk, O. N. Kazheva, A. N. Chekhlov and O. A. Dyachenko, *Org. Biomol. Chem.*, 2011, **9**, 1887.
59. K. Osakama, M. Sugiura, M. Nakajima and S. Kotani, *Tetrahedron Lett.*, 2012, **53**, 4199-4201.
60. M. O'Hagan, W. J. Shaw, S. Raugei, S. Chen, J. Y. Yang, U. J. Kilgore, D. L. DuBois and R. M. Bullock, *J. Am. Chem. Soc.*, 2011, **133**, 14301.
61. J. A. Franz, M. O'Hagan, M.-H. Ho, T. Liu, M. L. Helm, S. Lense, D. L. DuBois, W. J. Shaw, A. M. Appel, S. Raugei and R. M. Bullock, *Organometallics*, 2013, **32**, 7034-7042.
62. S. Sabo-Etienne and B. Chaudret, *Chem. Rev.*, 1998, **98**, 2077-2091.
63. D. M. Heinekey and W. J. Oldham, Jr., *Chem. Rev.*, 1993, **93**, 913-926.
64. W. J. Oldham, Jr., A. S. Hinkle and D. M. Heinekey, *J. Am. Chem. Soc.*, 1997, **119**, 11028-11036.
65. F. Maseras, A. Lledós, E. Clot and O. Eisenstein, *Chem. Rev.*, 2000, **100**, 601-636.
66. P. Spies, G. Erker, G. Kehr, K. Bergander, R. Fröhlich, S. Grimme and D. W. Stephan, *Chem. Commun.*, 2007, 5072.
67. G. C. Welch and D. W. Stephan, *J. Am. Chem. Soc.*, 2007, **129**, 1880-1881.

68. S. Grimme, H. Kruse, L. Goerigk and G. Erker, *Angew. Chem. Int. Ed.*, 2010, **49**, 1402-1405.
69. T. A. Rokob, I. Bakó, A. Stirling, A. Hamza and I. Pápai, *J. Am. Chem. Soc.*, 2013, **135**, 4425-4437.
70. J. C. Lee, Jr., E. Peris, A. L. Rheingold and R. H. Crabtree, *J. Am. Chem. Soc.*, 1994, **116**, 11014-11019.
71. A. Caballero, F. A. Jalón and B. R. Manzano, *Chem. Commun.*, 1998, 1879-1880.
72. D. M. Camaioni, B. Ginovska-Pangovska, G. K. Schenter, S. M. Kathmann and T. Autrey, *J. Phys. Chem. A*, 2012, **116**, 7228-7237.
73. Based on calculated H positions in the X-ray structure.
74. R. Custelcean and J. E. Jackson, *Chem. Rev.*, 2001, **101**, 1963-1980.

Graphical Abstract:

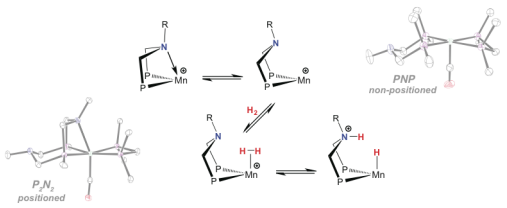

Table of Contents Entry:

A balance of metal electrophilicity and ligand steric influences is required for facile, reversible H–H heterolytic cleavage in Mn complexes with pendant amines.